Title	Broadband RF-Input Continuous-Mode Load-Modulated Balanced Power Amplifier With Input Phase Adjustment
Authors(s)	Pang, Jingzhou; Chu, Chenhao; Li, Yue; Zhu, Anding
Publication date	2020-10
Publication information	IEEE Transactions on Microwave Theory and Techniques, 68 (10): 4466-4478
Publisher	IEEE
Item record/more information	http://hdl.handle.net/10197/12018
Publisher's statement	© 2020 IEEE. Personal use of this material is permitted. Permission from IEEE must be obtained for all other uses, in any current or future media, including reprinting/republishing this material for advertising or promotional purposes, creating new collective works, for resale or redistribution to servers or lists, or reuse of any copyrighted component of this work in other works.
Publisher's version (DOI)	10.1109/tmtt.2020.3012141

Broadband RF-Input Continuous Mode Load Modulated Balanced Power Amplifier With Input Phase Adjustment

Jingzhou Pang, *Member, IEEE,* Chenhao Chu, *Student Member, IEEE,* Yue Li, *Student Member, IEEE,* and Anding Zhu, *Senior Member, IEEE*

***Abstract*—This paper presents the theory and design methodology of broadband RF-input continuous mode load modulated balanced power amplifier (CM-LMBA) by introducing the continuous mode output matching networks in the LMBA architecture. It is illustrated that the continuous mode impedance condition can be achieved by properly adjusting the phase difference between the different PA branches in the proposed CM-LMBA during the entire load modulation process. An RF-input CM-LMBA with 1.45-2.45 GHz bandwidth using commercial GaN transistors is designed and implemented to validate the proposed architecture. The fabricated CM-LMBA attains a measured 11.2-13.4 dB gain and around 40 Watts saturated power. Power added efficiency (PAE) of 46.4-56.5% and 43.2-50.3% is achieved at 6 dB and 8 dB output power back-off throughout the designed band. When driven by a 100 MHz OFDM signal with 8 dB peak to average power ratio (PAPR), the proposed CM-LMBA achieves better than -46 dBc adjacent channel leakage ratio (ACLR) and higher than 45% average PAE after digital pre-distortion at 1.8 GHz and 2.1 GHz.**

***Index Terms*—5G, broadband, continuous mode, high efficiency, LMBA, load modulation, power amplifier.**

I. Introduction

POWER amplifier (PA) is one of the most important components in modern wireless communication systems since it plays a critical role in affecting efficiency, linearity and bandwidth performance of the system [1]–[3]. Over the past decades, with the rapid development of wireless communication standards, bandwidth extension of high-efficiency PAs becomes one of the most popular topics in PA research, responding to the demand of supporting multi-band/multi-mode operation. Among the published bandwidth extension solutions for PAs, the continuous mode technique has received wide attentions since it provides a systematic design methodology for realizing high-efficiency broadband PAs from theory to practice. Continuous mode PAs have been implemented in various classes, e.g., continuous class B/J [2] and continuous class F/F^{-1} [4].

Modern wireless systems commonly employ modulated signals with high peak to average ratio (PAPR) to optimize utilization of the scarce spectrum resources, which creates strong demands for PAs with high efficiency performance at back-off. Many PA architectures, such as Doherty power amplifier (DPA), envelope tracking and out-phasing, have been introduced to improve the PA efficiency at output power back-off (OBO). Among them, the DPA possesses high reliability and low complexity, making it become the most widely used architecture in cellular base-stations. It is inevitable that the architecture of DPAs has been modified to achieve wider bandwidth over the past decade. By introducing techniques such as post-matching [5]–[12], complex combining loads [13], [14], modified load modulation network [15], [16] and dual-mode operation [17], [18], the bandwidth of the DPA has been greatly extended. Recently, some new PA architectures with high back-off efficiency and broadband feature have also been presented with novel load modulation operation, such as the load modulated balanced power amplifiers (LMBAs) [19]–[26] and distributed efficiency amplifiers (DEPAs) [27], [28]. Nevertheless, most of these techniques only focus on the fundamental impedance conditions, the high efficiency performance of the DPAs might not be guaranteed in the entire designed band.

It is attractive to introduce the continuous mode technique in high back-off efficiency PA architectures, because the continuous mode solution provides not only the possibility of bandwidth extension but also the flexible high efficiency design space. However, there are only few studies to date to explore this interesting topic. In [29] and [30], efforts have been done to combine the continuous mode technique and Doherty architecture by introducing modified load modulation networks (LMNs). However, for the continuous mode DPAs (CM-DPAs) in [29] and [30], only back-off impedance can satisfy the continuous mode requirement throughout the design bandwidth. When the output power is gradually increased, the fundamental impedance of the reported CM-DPAs will degenerates into class-B condition correspondingly. This feature reduces the in-band consistency of the CM-DPAs and also could decrease the efficiency performance to some extent in the Doherty power region. It is difficult to solve this problem because the requirements of load modulation and continuous mode impedance might be contradictory in the DPA operation. The mutual influence between the LMN and output matching networks (OMNs) further increases the difficulty. For the same reason, it is also difficult to introduce the continuous mode technique into out-phasing or DEPA architectures.

This work was supported in part by the Science Foundation Ireland under Grant Numbers 13/RC/2077, 17/NSFC/4850 and 16/IA/4449. This research was also funded in part by funding from the European Union's Horizon 2020 Research and Innovation Program under the Marie Sklodowska-Curie grant agreement number 713567. (*Corresponding author: Jingzhou Pang*)

The authors are with the School of Electrical and Electronic Engineering, University College Dublin, D04 E4X0 Dublin, Ireland.(e-mail: jingzhou.pang@foxmail.com; chenhao.chu@ucdconnect.ie; yue.li1@ucdconnect.ie; anding.zhu@ucd.ie)

Different from the above various architectures, load modulation in LMBAs is realized by injecting a control signal to a balanced PA pair. This configuration provides the possibility of designing the LMNs and OMNs relatively independently while maintaining the effective load modulation operation. This makes it easier to realize the continuous mode load modulation in LMBAs. However, as a relatively new technique, this feature has not been thoroughly studied and utilized. For example, the reported broadband LMBAs in [20]–[22] do not employ complete OMNs in the balanced PA. The reported RF-input LMBA in [23], sequential-LMBA (SLMBA) in [31] and phase controlled LMBA in [32] employ OMNs while the bandwidth performance and impact from the OMNs have not been analyzed in detail. In [33], the proposed Pseudo-Doherty LMBA (PD-LMBA) employs OMN for the carrier PA with similar system configuration to the SLMBA in [31] and achieves 57% fractional bandwidth with 10 dB OBO level, verified the feasibility of using OMNs in broadband LMBA-like architectures. The RF-input LMBA introduced in [23] has proven that Doherty-like operation can be achieved by the LMBA with RF-input structure. It is thus interesting to explore the possibility of bandwidth enhancement in RF-input LMBA structures by using the continuous mode output matching networks (CM-OMNs) while maintaining the Doherty-like performance.

In this paper, we proposed a novel RF-input LMBA architecture which employs the CM-OMNs. It is illustrated that the continuous mode impedance condition can be achieved by properly adjusting the phase difference between the different PA branches in the proposed CM-LMBA during the entire load modulation process. By employing different continuous mode load modulation at different operation frequencies, broadband CM-LMBA can be successfully realized. A broadband RF-input CM-LMBA using commercial GaN transistors is then designed and fabricated to validate the proposed architecture. The implemented CM-LMBA presents excellent efficiency performance within a broad bandwidth.

The remaining part of the paper is organized as follows, Section II presents the theory of the proposed RF-input CM-LMBA. Section III shows the detailed procedures of realizing the CM-LMBA with commercial GaN transistors on a 31 mil Rogers 5880 substrate. In Section IV, the experimental results are presented with a conclusion given in Section V.

II. Theoretical Analysis

The original LMBA described in [19] is a dual-input PA system based on balanced PA pair with injected control signal. It has been illustrated that active load modulation can be performed for the balanced PA pair by adjusting the amplitude and phase of the control signal. By properly changing the control signal characteristic at different operation frequencies, LMBAs can achieve high efficiency performance at the OBO throughout broad bandwidth. The original LMBA has been generalized to the RF-input architecture in [20] and [23] by using a control amplifier as the control signal source, especially achieves the Doherty-like performance in [23]. As mentioned earlier, the continuous mode operation has the potential to extend the bandwidth of RF PA with high-efficiency performance but it has not been fully exploited in LMBA design to date. In this paper, CM-OMNs are introduced in the balanced PA pair to improve the efficiency performance while maintaining broadband characteristic of the LMBA.

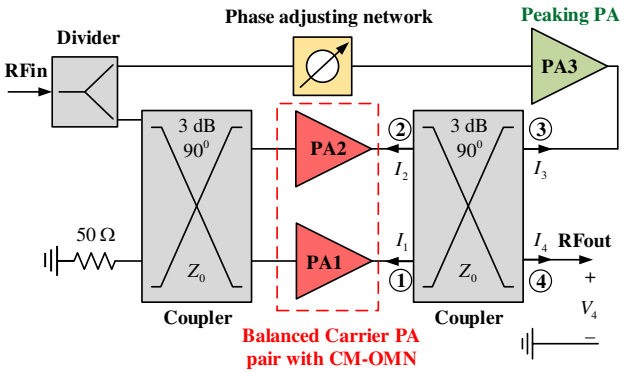

Fig. 1. Proposed RF-input CM-LMBA architecture.

A. RF-Input CM-LMBA Architecture

Fig. 1 presents the proposed RF-input CM-LMBA architecture. In this architecture, two class-B biased PAs with CM-OMNs are used as the carrier balanced PA pair. A class C biased PA is employed to realize the function of the control signal as the peaking PA. The peaking PA is turned off at the OBO, meanwhile, the carrier PAs are matched to required continuous mode impedance with high resistance to provide high back-off efficiency. When the peaking PA turns on, load modulation is performed for the carrier PAs to continuous mode impedance with smaller resistance, making the carrier PA generate more power while maintaining high efficiency status. The phase adjusting network provides the required phase relationship between the carrier and peaking PAs. Unlike other LMBA architectures, CM-OMNs are employed in the proposed LMBA to provide continuous mode operation, which makes the load modulation process become different.

The same as that in the original LMBA architecture, the voltage and current relationship at the four ports of the proposed CM-LMBA output coupler can be expressed as,

$$\begin{bmatrix} V_1 \\ V_2 \\ V_3 \\ V_4 \end{bmatrix} = Z_0 \begin{bmatrix} 0 & 0 & -j\sqrt{2} & -j \\ -j & -j\sqrt{2} & 0 & 0 \\ -j\sqrt{2} & -j & 0 & 0 \\ 0 & 0 & -j & -j\sqrt{2} \end{bmatrix} \begin{bmatrix} I_1 \\ I_2 \\ I_3 \\ I_4 \end{bmatrix} \quad (1)$$

where Z_0 is the reference impedance of the output coupler. Assume $I_1 = -jI_{ba}$, $I_2 = -I_{ba}$ and $I_3 = -jI_{pk}e^{j\phi_{pk}}$, we can obtain the modulated impedance at port 1 and port 2 as,

$$Z_1 = Z_2 = Z_{ba} = Z_0(1 - \sqrt{2}\frac{I_{pk}}{I_{ba}}e^{j\phi_{pk}}). \quad (2)$$

where ϕ_{pk} is the added current phase difference between port 3 and port 2. Meanwhile, the impedance at port 3 Z_{pk} keeps constant to Z_0.

At OBO, because $I_{pk} = 0$, it is obvious that $Z_{ba,obo} = Z_0$. In this situation, there is no difficulty for matching Z_0 to the required continuous mode impedance within a broad bandwidth

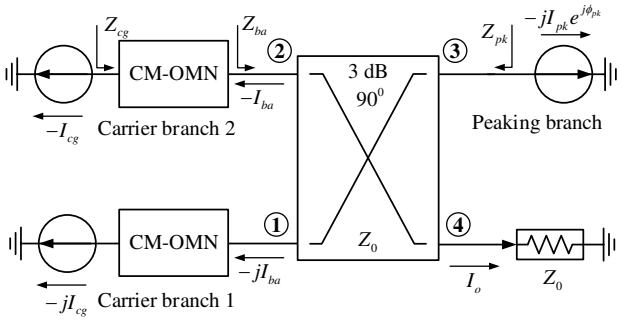

Fig. 2. Theoretical block diagram of the CM-LMBA.

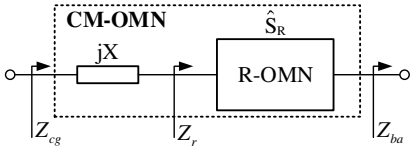

Fig. 3. Equivalent network of CM-OMN.

by using any reported CM-OMNs. This means the proposed architecture can easily achieve high back-off efficiency at OBO within broad bandwidth. However, when the peaking PA turns on, the used CM-OMN will affect the load modulation process of the LMBA. It is necessary to discuss the operation of the load modulation in the proposed CM-LMBA in detail.

B. Load Modulation in CM-LMBA With Input Phase Adjustment

To analyze the load modulation process of the proposed CM-LMBA, the theoretical block diagram shown in Fig. 2 is introduced here. In this configuration, the active devices are represented by three ideal current generators (CGs). We will use the class B/J continuum as the example to illustrate the load modulation in CM-LMBA. Let's assume the optimal class-B impedance of the carrier CGs is $R_{opt,c}$ at saturation. The corresponding impedance of the continuous class-B/J mode should be $R_{opt,c}(1+j\cdot\alpha)$, where α is the parameter related to different voltage waveform and $-1\leq\alpha\leq 1$ [2], [30]. To obtain high back-off efficiency, the proposed CM-LMBA should provide larger impedance at the carrier CG plane at OBO while maintaining the continuous mode feature. The required fundamental carrier impedance at CG plane Z_{cg} can be expressed as,

$$\begin{cases} Z_{cg,obo} = \beta R_{opt,c}(1+j\cdot\alpha) \\ Z_{cg,sat} = R_{opt,c}(1+j\cdot\alpha) \end{cases} \tag{3}$$

where β is defined as the impedance ratio between OBO and saturation at the carrier CG plane.

As mentioned in the previous subsection, at OBO, $Z_{ba,obo} = Z_0$. Therefore, the CM-OMN in Fig. 2 should match Z_0 to $\beta R_{opt}(1+j\cdot\alpha)$. When the peaking PA turns on, Z_{ba} will be modulated based on (2). To simplify the analysis of the continuous mode load modulation process, we use an equivalent network shown in Fig. 3 to represent the CM-OMN.

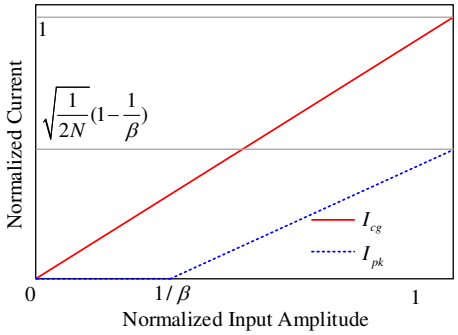

Fig. 4. Carrier and peaking current relationship of the proposed CM-LMBA.

This equivalent network consists of a real to real matching network R-OMN and a series reactance component. To provide the same continuous mode impedance at OBO, R-OMN should match Z_0 to $\beta R_{opt,c}$ and the added reactance value X should be $\alpha\beta R_{opt,c}$. In this situation, the required impedance at the matching port of R-OMN should be,

$$\begin{cases} Z_{r,obo} = \beta R_{opt,c} \\ Z_{r,sat} = R_{opt,c}(1-j\cdot(\beta-1)\alpha) \end{cases} \tag{4}$$

The related reflection coefficient at saturation can be calculated as,

$$\Gamma_{r,sat} = \frac{Z_{r,sat}-Z_{r,obo}}{Z_{r,sat}+Z_{r,obo}}. \tag{5}$$

Substituting (4) into (5) we can obtain,

$$\Gamma_{r,sat} = \frac{(1-\beta)\sqrt{1+\alpha^2}\cdot e^{j\arctan\alpha}}{2\beta-(\beta-1)\sqrt{1+\alpha^2}\cdot e^{j\arctan\alpha}}. \tag{6}$$

At OBO, R-OMN is matched at both ports. Assuming R-OMN is a lossless network, the S parameter matrix of it can be expressed as,

$$\hat{\mathbf{S}}_{\mathbf{R}} = \begin{bmatrix} 0 & e^{j\phi_r} \\ e^{j\phi_r} & 0 \end{bmatrix} \tag{7}$$

where ϕ_r is the phase shift of R-OMN. Based on the method in [30], [34], at saturation, the required reflection coefficient at the coupler port 1 and 2, Γ_{ba} can be calculated as,

$$\Gamma_{ba,sat} = \Gamma_{r,sat}\cdot e^{-j2\phi_r}. \tag{8}$$

Substituting (6) into (8), we obtain

$$\Gamma_{ba,sat} = \frac{(1-\beta)\sqrt{1+\alpha^2}\cdot e^{j(\arctan(\alpha)-2\phi_r)}}{2\beta-(\beta-1)\sqrt{1+\alpha^2}\cdot e^{j\arctan(\alpha)}}. \tag{9}$$

Meanwhile, Γ_{ba} can be also expressed as

$$\Gamma_{ba,sat} = \frac{Z_{ba,sat}-Z_0}{Z_{ba,sat}+Z_0}. \tag{10}$$

Based on (2), to obtain the calculation of (10), the relationship between I_{pk} and I_{ba} can be found out.

In [19], the current magnitude relationship without OMNs is given. It should be noticed that CM-OMN provides a specific impedance transformation ratio while different continuous mode impedance provides same output power ability. Therefore, based on the analysis in [19], the normalized

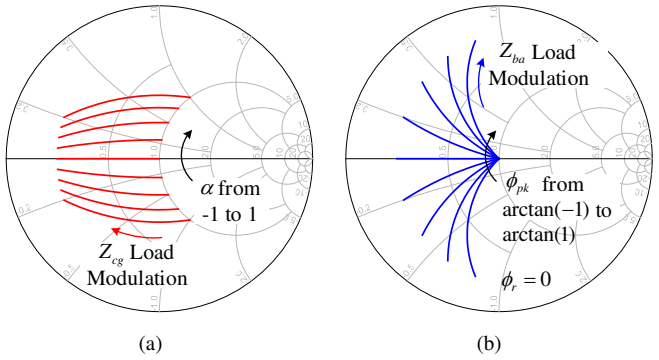

Fig. 5. Load modulation of Z_{cg} and Z_{ba} when $\phi_r = 0$ on Smith chart with reference impedance of $\beta R_{opt,c}$: (a) Z_{cg} and (b) Z_{ba}.

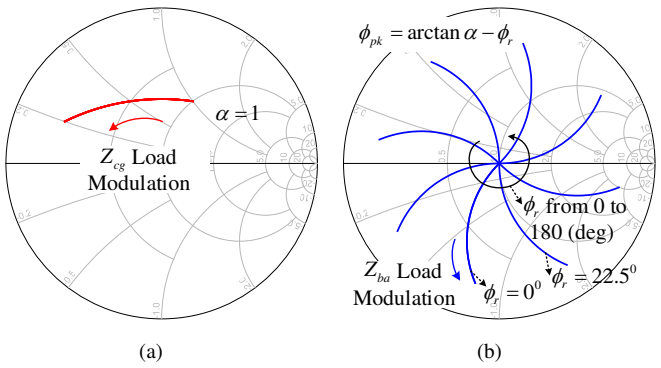

Fig. 6. Load modulation example of Z_{cg} and Z_{ba} when $\alpha = 1$ and $\phi_r \neq 0$ on Smith chart with reference impedance of $\beta R_{opt,c}$: (a) Z_{cg} and (b) Z_{ba}.

current relationship between the peaking and carrier CGs in the proposed architecture can be simply modified as follows,

$$\sqrt{N} \cdot I_{pk} = \begin{cases} 0, & 0 \leq I_{cg} < \dfrac{1}{\beta} \\ \dfrac{1}{\sqrt{2}}(I_{cg} - \dfrac{1}{\beta}), & \dfrac{1}{\beta} \leq I_{cg} \leq 1. \end{cases} \tag{11}$$

where N is the real to real impedance transformation ratio of the CM-OMN, which can be expressed as,

$$N = \frac{Z_0}{\beta R_{opt,c}} \tag{12}$$

Fig. 4 presents the normalized carrier and peaking current relationship.

According to (11), the normalized peaking current at saturation can be expressed as,

$$I_{pk,sat} = \frac{1}{\sqrt{2N}}(1 - \frac{1}{\beta}) \tag{13}$$

Besides, based on the feature of the lossless two-port network we can obtain the normalized balanced current as,

$$I_{ba,sat} = \frac{1}{\sqrt{N(1+\alpha^2)}}(e^{-j\phi_r} - j(\frac{1}{\beta} - 1)(1 + j\alpha)\sin\phi_r) \tag{14}$$

Therefore, according to (2), (10), (13) and (14) we can obtained the following expression,

$$\Gamma_{ba,sat} = \frac{(1-\beta)\sqrt{1+\alpha^2} \cdot e^{j(\phi_{pk} - \phi_r)}}{2\beta - (\beta - 1)\sqrt{1+\alpha^2} \cdot e^{j\arctan(\alpha)}}. \tag{15}$$

From (9) and (15) we can know, to achieve the required carrier continuous mode impedance at saturation, the following phase relationship should be satisfied,

$$\phi_{pk} = \arctan(\alpha) - \phi_r. \tag{16}$$

Equation (16) indicates that the required continuous mode load modulation can be achieved by introducing phase adjustment element in front of the peaking branch to satisfy this phase relationship.

Using the similar method, it can be proven that, when (11) and (16) are both satisfied, the continuous mode impedance condition will be achieved at the carrier CG plane during the entire load modulation process. Fig. 5 shows the load modulation of Z_{cg} and Z_{ba} when $\phi_r = 0$ as an example on the Smith chart. The reference impedance of the Smith chart is set to $\beta R_{opt,c}$. It can be seen that, for different value of α, the load modulation of Z_{ba} is different. Nevertheless, once we adjust the phase ϕ_{pk} to satisfy the condition $\phi_{pk} = \arctan(\alpha)$, the corresponding continuous mode load modulation can be correctly achieved at the carrier CG plane.

Fig. 6 shows the load modulation of Z_{cg} and Z_{ba} for different ϕ_r. Due to the similarity of feature, only the situation when $\alpha = 1$ is given in Fig. 6. The reference impedance of the Smith chart is also set to $\beta R_{opt,c}$. It can be seen that, the required load modulation curve of Z_{ba} undergoes phase deflection as the value of ϕ_r changes. Nevertheless, regardless of how the load modulation curve of Z_{ba} is deflected, as long as the condition (16) is satisfied, the continuous mode load modulation of Z_{cg} does not change.

From the above analysis we can see that, the phase adjustment of the proposed CM-LMBA is dependent on the specific continuous mode impedance value and the phase shift of R-OMN ϕ_r. It should be noticed that, the physical meaning of ϕ_r is the phase shift of the CM-OMN when its two ports are in perfect match. We can directly obtain the required adjusting phase by measuring the phase of a practical CM-OMN. However, both carrier and peaking PAs employ OMNs in practical designs, so it is difficult to give an accurate value of the required ϕ_{pk} based on practical network phase relationship. It is thus more feasible to obtain the target phase relationship between the carrier and peaking PAs for adjusting ϕ_{pk} by employing the dual-input architecture or circuits simulation method in the practical design, and then design a phase adjustment network to provide this required phase in the front of the peaking PA as the structure shown in Fig.1.

It should be noticed that, for the peaking PA, it is theoretically easier to realize the continuous mode operation because there is no load modulation process at the isolation port of the output coupler. Therefore, for the proposed CM-LMBA architecture, continuous mode operation can be built for both the carrier and peaking PA, and thus broadband and high efficiency performance will be easier to achieve.

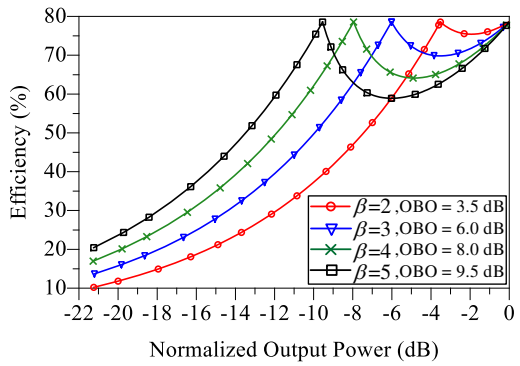

Fig. 7. Theoretical efficiency of the proposed CM-LMBA versus OBO levels for different values of β.

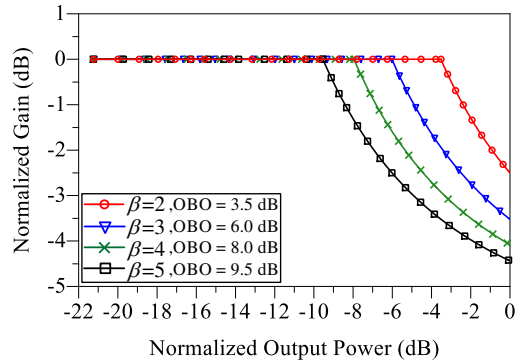

Fig. 8. Theoretical gain of the proposed CM-LMBA versus OBO levels for different values of β.

C. Theoretical Performance of the CM-LMBA

Because the continuous mode impedance does not affect the output power, the output power of the proposed CM-LMBA at OBO and saturation can be calculated as,

$$\begin{cases} P_{out,obo} = \dfrac{2}{\beta} R_{opt,c} \\ P_{out,sat} = 2R_{opt,c} + \dfrac{1}{2}(1-\dfrac{1}{\beta})^2 \beta R_{opt,c} \end{cases} \tag{17}$$

Therefore, the OBO level of the proposed CM-LMBA can be calculated as,

$$\text{OBO} = \frac{P_{out,sat}}{P_{out,obo}} = \beta + \frac{(\beta-1)^2}{4} \tag{18}$$

From (18) we can see, that the CM-LMBA presents different OBO levels for different values of β.

It should be noticed that for the continuous mode class B/J PA, the efficiency performance is the same as the class B mode no matter which specific impedance is used. Because the continuous mode impedance condition is always satisfied throughout the entire load modulation process for the proposed CM-LMBA, the ideal efficiency will be the same as the situation when $\alpha = 1$. Fig. 7 presents the efficiency of the proposed CM-LMBA versus OBO levels for different values of β. It can be seen that, when β changes from 2 to 5, the OBO level is extended from 3.5 dB to 9.5 dB.

Fig. 8 shows the theoretical gain of the proposed CM-LMBA versus OBO levels for different values of β. It can be seen that, as the level of OBO increases, the gain compression becomes larger. The gain compression is caused by the load modulation of the carrier PA, as the carrier impedance becomes smaller with the increase of the driven power level. It is worth to mention that, the gain compression results shown in Fig. 8 are based on the ideal linear voltage controlled current source model. In practical active devices, the gain compression may not be as severe as that in theory and thus the linearity of fabricated CM-LMBAs could be better than that predicted in the theory.

D. Harmonic Impedance Control

The above subsections illustrate the fundamental load modulation process of the proposed CM-LMBA, it is assumed that the required harmonic impedance condition has been satisfied throughout the load modulation process. To ensure the efficiency performance at OBO, the CM-OMN should be designed to satisfy the second harmonic impedance condition of the corresponding continuous mode as follows,

$$Z_{cg,obo}[2] = \beta R_{opt,c}(-j\frac{3\pi}{8}\cdot\alpha). \tag{19}$$

It is relatively easy to achieve this required second harmonic impedance condition at OBO, guaranteeing the corresponding continuous mode operation. However, it is difficult to avoid mismatch of the second harmonic impedance for the carrier PA when the output power is higher than the back-off level. Nevertheless, this kind of mismatch would not make the performance of the proposed CM-LMBA drop so much. Firstly, the condition (19) ensures that the second harmonic impedance is pure reactance while the non-zero resistance of the second harmonic impedance has a greater impact on the performance [35]. Secondly, the closer to the back-off region, the less obvious the mismatch. In [35], the impact on the efficiency from the mismatch of the second harmonic impedance of continuous class B/J mode was discussed. When considering the pure reactance situation, the ideal efficiency will not drop by more than 5% even if the mismatch deviation of second harmonic reactance reaches $\pm 0.5\alpha$. Based on the LMBA theory, there is no load modulation for the peaking PA, thus the second harmonic impedance of the peaking PA should be constant throughout the whole output power range. Therefore, it should be easier to design the peaking OMN which can provide the required peaking second harmonic impedance.

III. Design of the Proposed CM-LMBA

To validate the proposed architecture, an RF-input CM-LMBA using GaN transistors was designed and fabricated, the target bandwidth was 1.5-2.5 GHz. Commercial GaN HEMTs CGH40010F from Wolfspeed were used as active devices for the carrier PAs. R_{opt} of the used transistor was 32 Ω for class B operation [9], [30]. The designed CM-LMBA was realized on a 31 mil thick Rogers 5880 substrate with the dielectric constant of 2.2. In the design, $\beta = 4$ was chosen to provide

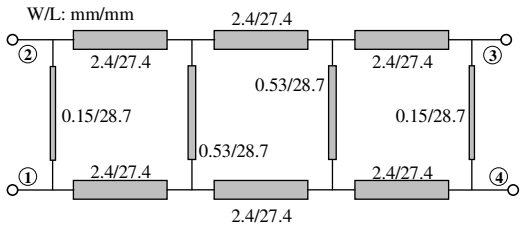

Fig. 9. Schematic of the designed broadband coupler.

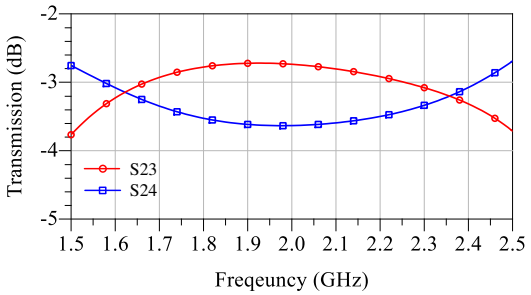

(a)

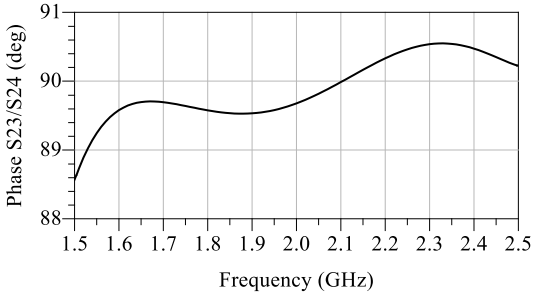

(b)

Fig. 10. EM-Simulated characteristic of the designed broadband coupler (a) transmission (b) phase difference between port 2 and port 4.

8 dB OBO. For this configuration, we could obtain $N = 0.39$ and $I_{pk,sat} = 0.85I_{cg,sat}$ based on (11) and (12). In this configuration, the power ratio between the peaking and one carrier branch ccould be calculated as $(50I^2_{pk,sat})/(32I^2_{cg,sat}) = 1.12$. Because the maximum peaking power was so close to the carrier one, CGH40010F was then also chosen as the peaking active device.

It was necessary to firstly design a broadband coupler for the balanced PA pair at both the input and output of each carrier continuous mode PA. Fig. 9 presents the schematic of the designed broadband coupler, multi-stage branch line structure was employed to achieve the target bandwidth. Fig. 10 shows EM-simulated S-parameter characteristic of the designed coupler. It can be seen that the designed coupler effectively provides the required phase difference between port 3 and port 4 with less than 2 degree fluctuation while the transmission characteristic are deviated from the ideal value. The input and output couplers employed the same structure.

After designing the broadband coupler, a CM-OMN was designed to achieve the required conitinuous mode impedance at OBO for the two carrier branches. Fig. 11 presents the cir-

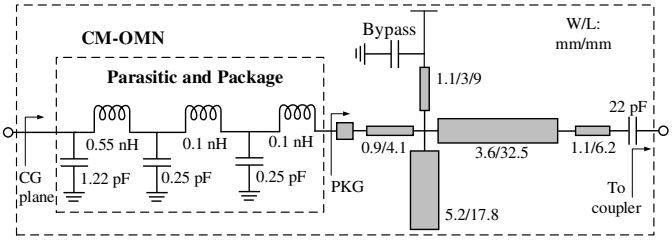

Fig. 11. Schematic of the designed CM-OMN.

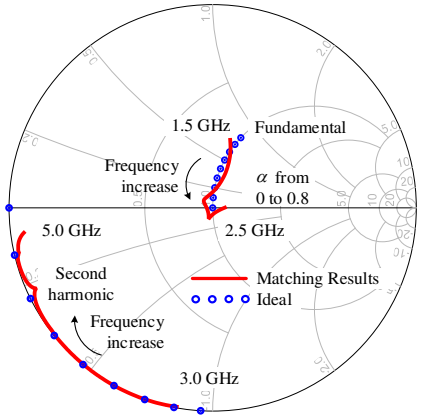

Fig. 12. Simulated matching results of the designed CM-OMN from 1.5 GHz to 2.5 GHz on Smith chart with reference impedance of βR_{opt}.

cuits details of the designed CM-OMN. Because the required continuous mode impedance should be obtained at the CG plane, the parasitic and package components were absorbed in this designed CM-OMN. The specific values of the parasitic and package components were obtained from the de-embeded transistor model introduced in [9]. It should be noticed that, the specific circuit structure of the CM-OMN would not affect the operation of the CM-LMBA and the design method of CM-OMNs have been presented in many publications [4], [35]–[38], so we would not discuss how to design the CM-OMN in detail in this paper. A simplified transmission line (TL) structure of the matching network introduced in [18] was used to obtain the specific value of the designed CM-OMN as shown in Fig. 11. For the carrier branch, the matching results within the designed band at the CG plane was presented on the Smith chart in Fig. 12, where the reference impedance of this Smith chart was set to βR_{opt}. It can be seen that, both the fundamental and second harmonic matching results are close to the ideal continuous Class B/J impedance. The structure of the peaking OMN (POMN) was similar to the CM-OMN. As we early mentioned, there would be no load modulation in the peaking branch in theory, so the function of the POMN was directly matching the coupler reference impedance to the required peaking impedance at saturation. We will not discuss the POMN design here in detail.

Broadband input matching network (IMN) was then designed to ensure gain performance in the designed band. The carrier and peaking branch used the same IMN in this design. Stepped TL structure was used to design the IMN with a

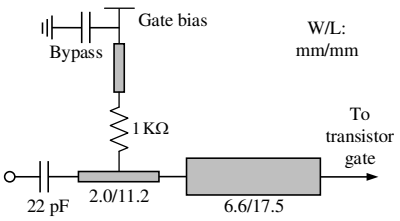

Fig. 13. Schematic of the designed input matching network.

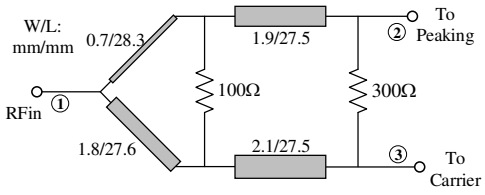

Fig. 14. Schematic of the designed broadband uneven divider.

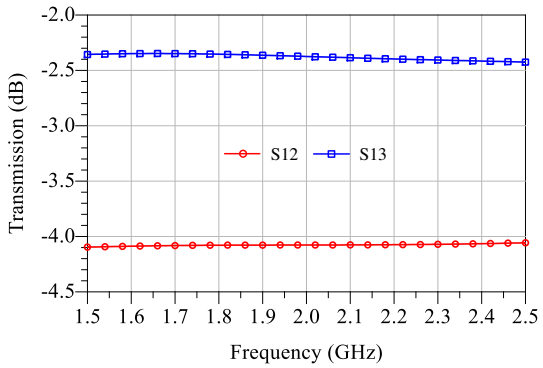

Fig. 15. Simulated transmission results of the designed broadband uneven divider.

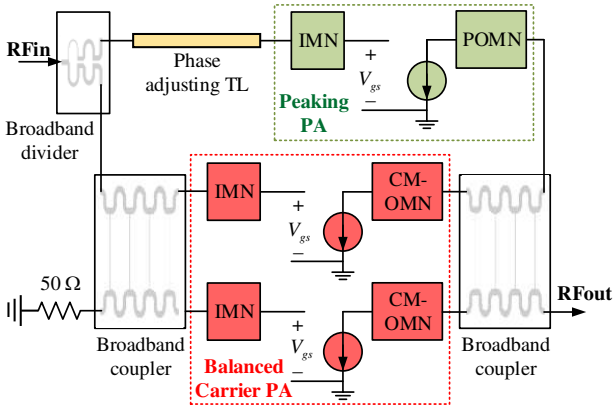

Fig. 16. Entire schematic of the proposed CM-LMBA.

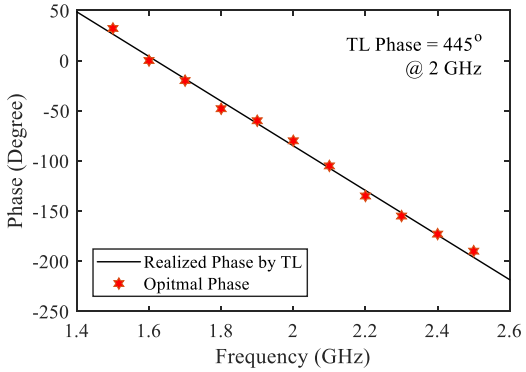

Fig. 17. Optimal phase shift between the carrier and peaking branches and the realized phase by TL.

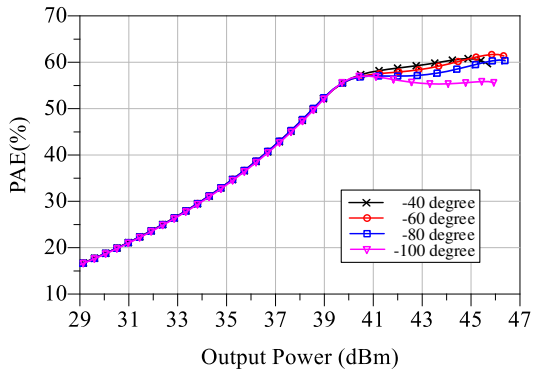

Fig. 18. Simulated PAE versus output power at 2.0 GHz with different input phase adjustment.

large resistance in the gate bias line. The specific value of the components in IMN is shown in Fig. 13. A two-stage broadband uneven power divider was designed to provide the required power distribution from 1.5 GHz to 2.5 GHz. The circuits detail of the designed power divider is shown in Fig. 14. It should be noticed that, the power distribution ratio between the carrier and peaking branches should be 2:1 based on the theoretical analysis. In practical design, this ratio was optimized to some extent to obtain better performance. The simulated transmission results of the designed broadband uneven divider for different ports are shown Fig. 15. It can be seen that, the designed divider provides almost constant power distribution ration throughout the target bandwidth.

After all the designs of the above functional parts of the proposed CM-LMBA, the required phase shift between the carrier and peaking branches should be obtained to ensure the load modulation process. An input phase adjustment network was thus required. In this design, a TL was added at the front of the peaking IMN as the phase adjustment network. Therefore, the entire schematic of the proposed CM-LMBA is as Fig. 16 shows. As we mentioned early, considering the phase shift introduced by the different matching networks and active device operation, it is better to obtain the required phase shift by adjusting it at different operation frequencies in simulation. We used an ideal phase shifter at the same position of the phase adjustment TL in Fig. 16. By adjusting the phase

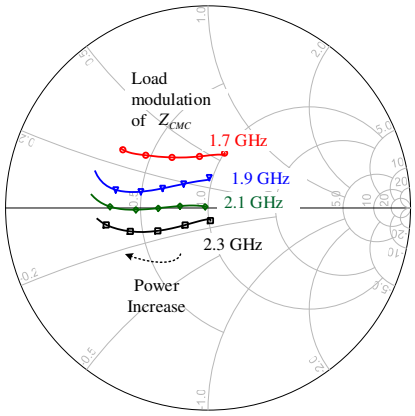

Fig. 19. Simulated load modulation of Z_{ba} at carrier CG plane.

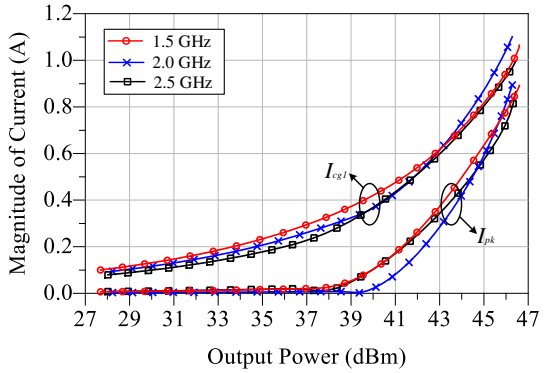

Fig. 20. Simulated carrier and peaking drain current versus output power at different operation frequencies.

shifter at different frequencies, the optimal phase shift between the carrier and peaking branches can be obtained based on the performance of the CM-LMBA as shown in Fig. 17.

After obtaining the optimal phase shift, a TL with phase shift of 445° at 2 GHz was then employed to fit the required phase shift within the designed band. The fitting results were plotted in Fig. 17. It can be seen that, the realized phase shift by the proposed TL approaches the obtained optimal phase value well at different frequencies. It should be noticed that, using a TL as the phase adjustment network is a specific case here. Sometimes TLs might not be able to fit the optimal phase well, because the phase slope and the reference phase at the centre frequency of a TL are fixed. Nevertheless, we believe that the optimal phase difference in a linear relationship with frequency can be achieved in many broadband matching network designs [17], [18]. Therefore, other circuit structures, such as that introduced in [18], can also be used as the phase adjustment network for the proposed CM-LMBA in more general cases. To verify how sensible the input phase shift affects the PA performance, the simulated PAE of the designed CM-LMBA at 2.0 GHz with different input phase adjustments is presented in Fig. 18, where the input phase shift changes from -40 degree to -100 degree with a step of 20 degrees. It can be seen that the phase shift has impact on the efficiency and power performance when the peaking PA turns on, but

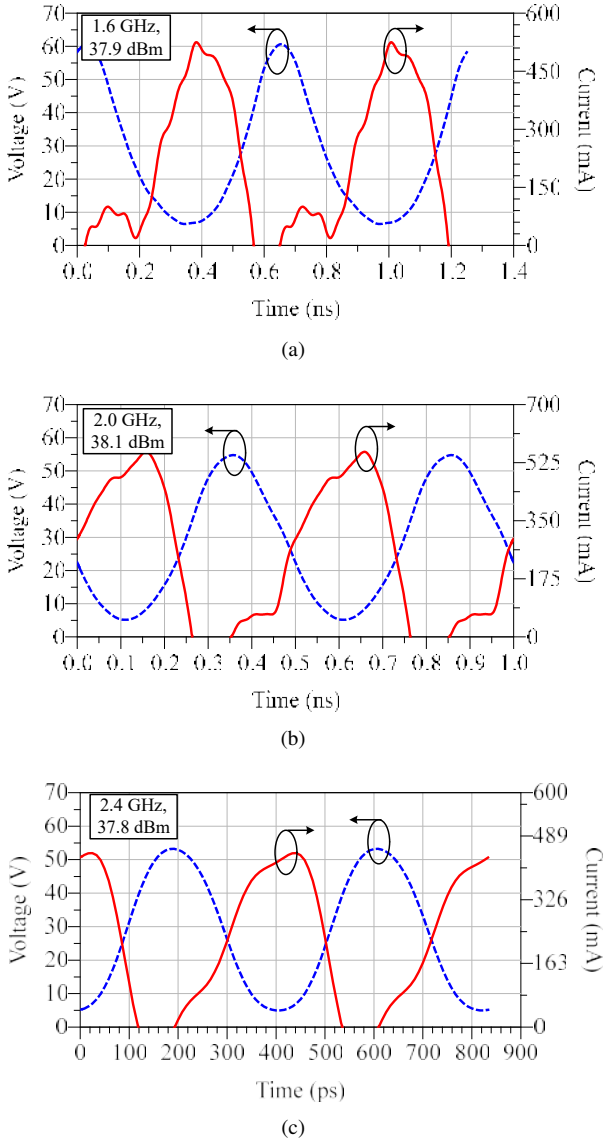

Fig. 21. Simulated drain voltage and current waveforms of one carrier PA at OBO: (a) waveform at 1.6 GHz with LMBA output power of 37.9 dBm, (b) waveform at 2.0 GHz with LMBA output power of 38.1 dBm and (c) waveform at 2.4 GHz with LMBA output power of 37.8 dBm .

the impact is relatively small considering that the achieved phase deviates by only a few degrees from the required optimal value.

After the above mentioned designs, the entire circuits of the designed CM-LMBA were then EM-simulated using Keysight ADS. Fundamental load modulation process at the carrier CG plane at some operation frequencies are shown in Fig. 19. We can see that, the simulated load modulation results are close to the ideal ones but there are also certain deviations at different power levels and frequencies. The deviations are caused by the non-ideal coupler design and imperfect phase adjustment. Fig. 20 shows the simulated carrier and peaking drain current versus the output power at 1.5 GHz, 2.0 GHz and 2.5 GHz. The plotted carrier current was obtained from one PA of the balanced PA pair. The saturated current ratio is close to the theoretical value. It can be seen, the current behaviour of the

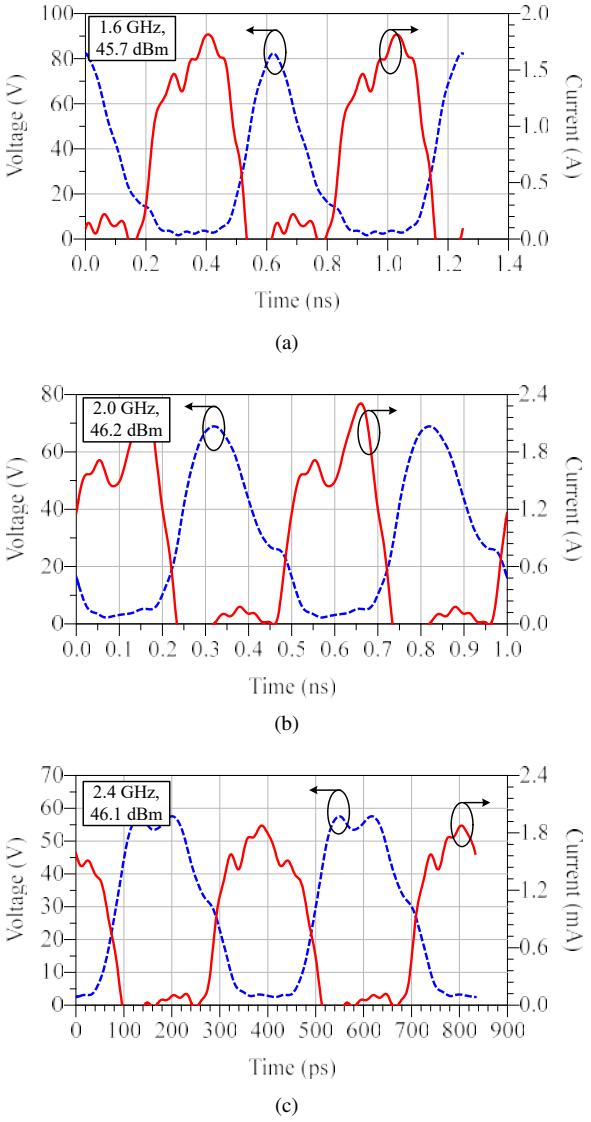

Fig. 22. Simulated drain voltage and current waveforms of one carrier PA at saturation: (a) waveform at 1.6 GHz with LMBA output power of 45.7 dBm, (b) waveform at 2.0 GHz with LMBA output power of 46.2 dBm and (c) waveform at 2.4 GHz with LMBA output power of 46.1 dBm .

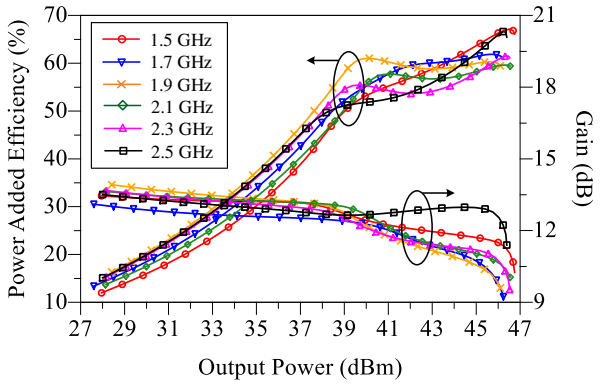

Fig. 23. Simulated PAE and gain versus output power at different operation frequencies.

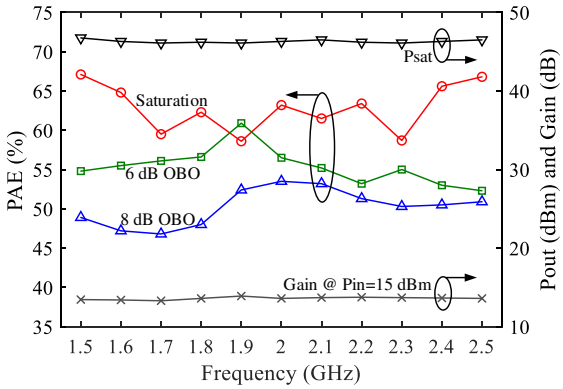

Fig. 24. Simulated PAE, output power and small signal gain versus frequency.

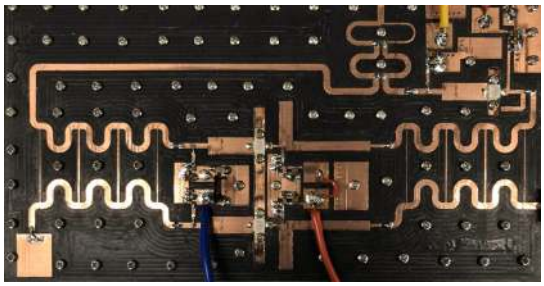

Fig. 25. Photograph of the fabricated CM-LMBA.

proposed CM-LMBA is close to the DPA. To better present the continuous-mode operation, the simulated drain voltage and current waveforms at some different operation frequencies and different output power levels are given in Fig. 21 and Fig. 22. All these waveforms were obtained at the CG plane. Fig. 21 presents the voltage and current waveforms at 1.6 GHz, 2.0 GHz and 2.4 GHz when the output power level of the CM-LMBA is close to 38 dBm. The related OBO level is about 8 dB. Fig. 22 presents the voltage and current waveforms at the same frequencies when the output power level is close to 46 dBm. From Fig. 21 and Fig. 22 we can see that, only a small part of the voltage and current waveforms overlap at both OBO and saturation, indicating the high efficiency performance of the designed CM-LMBA. Moreover, the voltage swing is larger at the lower frequency than the higher frequency, which is consistent with the continuous mode theory.

Fig. 23 shows the simulated PAE and gain of the design CM-LMBA versus the output power at different operation frequencies. It can be seen that back-off efficiency is obviously improved compared with single-ended PAs. Excellent back-off efficiency performance has been achieved. From 1.5 to 2.5 GHz, PAE of 58.6%-67.1%, 51.1%-60.9% and 46.8%-53.7% at saturation, 6 dB OBO and 8 dB OBO. To better present the broadband performance, the simulated performance at different frequencies are also given here in Fig. 24.

IV. Measurements Results

Fig. 25 presents the photograph of the fabricated CM-LMBA. Both continuous-wave (CW) and wideband modulated signals were employed to perform the measurements for the

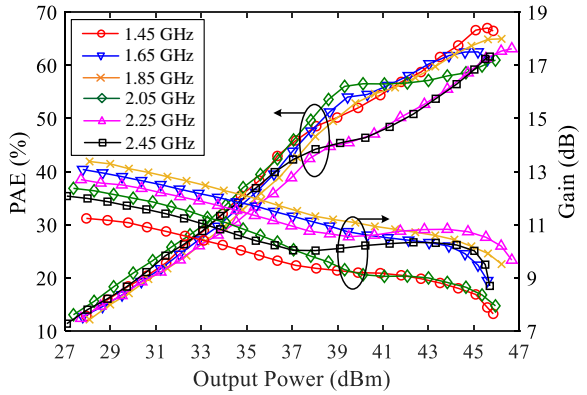

Fig. 26. Measured PAE and gain versus output power at different operation frequencies.

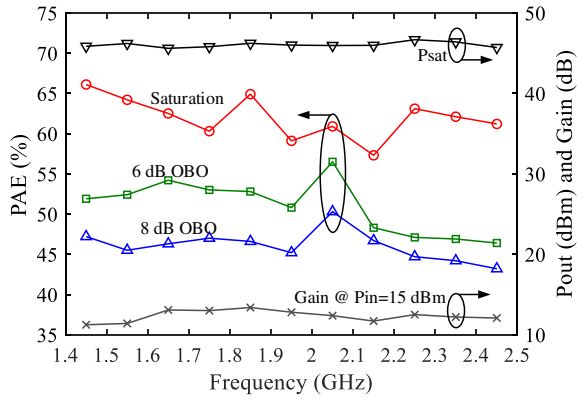

Fig. 27. Measured PAE, output power and small signal gain versus frequency with CW signal test.

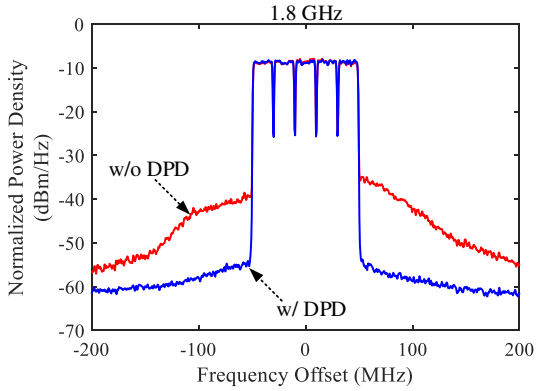

Fig. 28. Output spectrum of the proposed CM-LMBA at 1.8 GHz with and without DPD linearization.

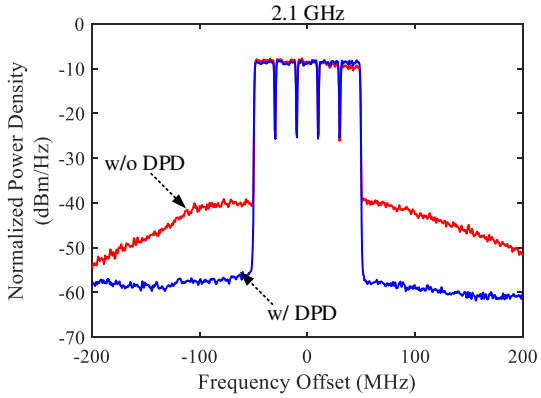

Fig. 29. Output spectrum of the proposed CM-LMBA at 2.1 GHz with and without DPD linearization.

fabricated CM-LMBA. The drain supply voltage of 28 V and total quiescent current of 160 mA for the balanced carrier PA pair were set during all the measurements. The drain voltage of the peaking PA was set to 34 V to ensure better linearity and the peaking bias voltage was set to -6 V. During the measurements, the employed CW and modulated signals were both generated by a vector signal generator (VSG), and the output power was measured using a spectrum analyzer. A broadband linear driver amplifier was used to drive the CM-LMBA with enough input power. A broadband circulator was added between the driver and CM-LMBA to improve isolation.

A. Measurements under CW Signal Stimulation

The fabricated CM-LMBA was firstly measured under CW signal stimulation at different operation frequencies with different input power levels. The realized frequency band of the CM-LMBA with high back-off efficiency performance slightly shifted due to the fabrication variations and the model inaccuracy of the transistors. The CM-LMBA was driven from low power region to saturation from 1.45 GHz to 2.45 GHz with 0.1 GHz step. Fig. 26 presents the measured PAE and gain versus output power at different operation frequencies. It can be seen that, Doherty-like behaviour was achieved by the implemented CM-LMBA within the designed frequency band. To better present the broadband performance, the measured PAE at different output power levels, output power at saturation and small signal gain versus the operation frequency were presented in Fig. 27. It appears that there is a certain degree of deviation between the measurements and simulations. This might be caused by the inaccuracy of the active device model especially that in the Class-C operation.

Within the realized bandwidth, the proposed CM-LMBA achieves peak PAE of 57.3%-66.1% with saturated output power of 45.6 dBm to 46.7 dBm, which is 36.3 Watts to 46.8 Watts. Back-off PAE of 46.4%-56.5% and 43.2%-50.3% are achieved throughout the entire operation band at 6 dB and 8 dB OBO, respectively. 11.2 dB to 13.4 dB gain is obtained at around 28 dBm output power level. The fractional bandwidth of the proposed CM-LMBA is 51.3%.

B. Measurements under Modulated Signal Stimulation

To evaluate the linearity and efficiency performance of the proposed CM-LMBA under modulated signals stimulation, a 5-carrier 100 MHz OFDM signal with 8 dB PAPR was used to test the CM-LMBA from 1.5 GHz to 2.4 GHz with 0.1 GHz step. The Magnitude-Selective Affine (MSA) function model based DPD method [41] was adopted to linearize the designed CM-LMBA. Fig. 28 and Fig. 29 present the output spectrum with and without DPD linearization under the stimulation of

TABLE I
PERFORMANCE COMPARISON OF RECENTLY PUBLISHED HIGH EFFICIENCY PAS.

Ref. (Year)	Technique N/A	Freq (GHz)	B. W. (GHz/%)	Pmax (dBm)	Gain (dB)	PAE@Sat. (%)	DE@Sat. (%)	OBO (dB)	PAE@OBO (%)	DE@OBO (%)
[20]2017	RF-input LMBA	1.8-3.8	2.0/71	42-44	11-12	37-59	N/A	6	29-45	N/A
[21]2018	Dual-input LMBA	1.7-2.5	0.8/38.1	48-48.9	9.9-13.2	48-58	N/A	6/ 8	43-53/ 39-50	N/A
[28]2019	DEPA	2.55-3.8	1.25/40	48.8-49.8	9.3-12.7	N/A	54-67	8	N/A	47-60
[29]2016	CM-DPA	1.65-2.75	1.1/50	44.5-46.3	9.3-11.7	N/A	66-77	6	N/A	52-66
[30]2018	CM-DPA	1.6-2.7	1.1/51	43.8-45.2	9.4-11.5	N/A	56-75.3	6	N/A	46.5-63.5
[31]2020	RF-input SLMBA	3.05-3.55	0.5/15.2	42.3-43.7	9.5-10.3	50.6-62.5	60.8-74.8	6/ 8/ 10	44.1-54.2/ 40.9-55.1/ 38.0-46.7	50.9-64.9/ 46.8-60.7/ 43.2-51.4
[39]2019	3-stage Doherty	1.6-2.6	1.0/47.6	45.5-46	8.5-11	N/A	53-66	9.5	N/A	50-53
[40]2019	Out-phasing	1.9	N/A	44	13	70	N/A	8	73	N/A
This work	RF-input CM-LMBA	1.45-2.45	1.0/51.3	45.6-46.7	11.2-13.4	57.3-66.1	67.1-77.9	6/ 8	46.4-56.5/ 43.2-50.3	51.2-64.4/ 47.8-55.7

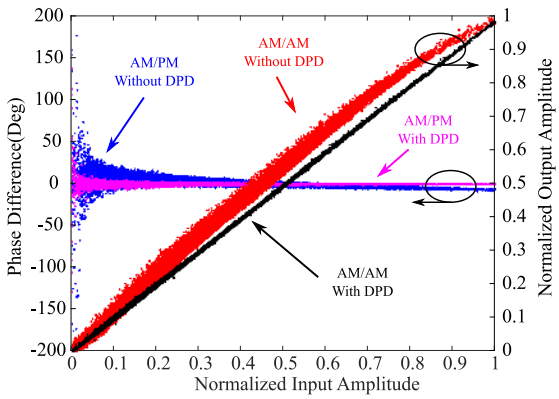

Fig. 30. AM-AM and AM-PM of the proposed CM-LMBA at 1.8 GHz with and without DPD linearization.

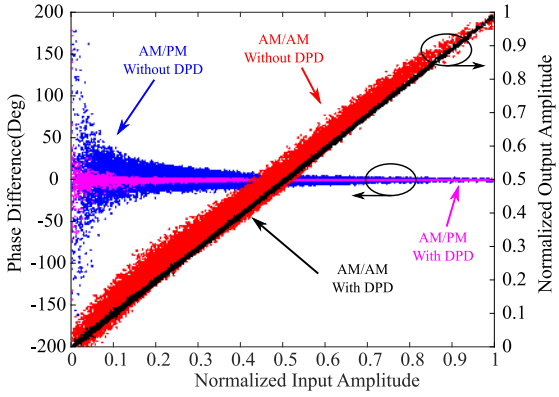

Fig. 31. AM-AM and AM-PM of the proposed CM-LMBA at 2.1 GHz with and without DPD linearization.

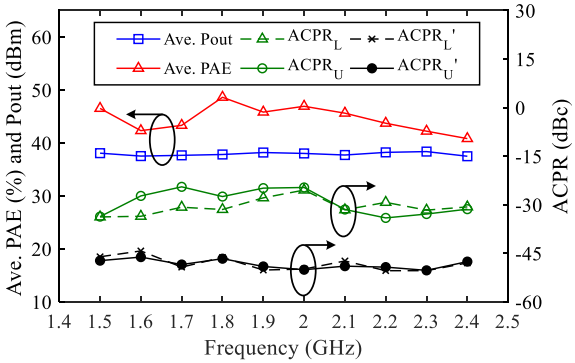

Fig. 32. Measured average PAE, output power and ACPR versus frequency with modulated signal test.

the employed 100 MHz signal at 1.8 GHz and 2.1 GHz, respectively. It can seen that, the linearity of the CM-LMBA was obviously improved after DPD.

The measured ACPRs of the CM-LMBA were -31.5/-27.5 dBc at 1.8 GHz and -31.6/-31.5 dBc at 2.1 GHz without DPD. After DPD was performed, the ACPRs were improved to -46.3/-46.7 dBc at 1.8 GHz and -47.4/-49.0 dBc at 2.1 GHz. Around 37.8 dBm average output power was achieved after DPD at these two frequencies with average PAE of 48.6% and 45.6%. The AM-AM and AM-PM characteristics with and without DPD are also given here in Fig. 30 and Fig. 31. It can be seen the nonlinearity can be corrected very well after the employed DPD performed.

Fig. 32 summarizes the measure average PAE, output power and ACPR performance from 1.5 GHz to 2.4 GHz under the 100 MHz modulated signal stimulation. ACPR_L and ACPR_U are the ACPR performance without DPD, ACPR'_L and ACPR'_U are the ACPR performance after DPD. Higher than 40% PAE was achieved by the CM-LMBA with averaged output power

of 37.5-38.2 dBm. Better than -24.5 dBc ACPR was obtained without DPD and improved to better than -44.3 dBc after DPD performed.

C. Performance Comparison

Table I summarizes the performance of some recently reported PAs with high back-off efficiency. Compared with other published high efficiency PAs, the proposed CM-LMBA shows excellent efficiency performance at both saturation and 6/8 OBO levels. At the same time, the proposed CM-LMBA achieves wider than 50% fractional bandwidth. Particularly, the proposed RF-input CM-LMBA shows higher efficiency than other reported LMBAs while maintaining broadband performance. When compared with DPAs which also employ the continuous mode technique, higher gain and larger OBO level were achieved by the proposed CM-LMBA with comparable efficiency performance.

V. Conclusion

The theory and implementation of the RF-input CM-LMBA was presented in this paper. Continuous mode technique was introduced in the LMBA architecture to improve the efficiency performance while maintaining broadband feature. The realized CM-LMBA presents excellent back-off PAE with 51.3% fractional bandwidth. Meanwhile, from the results of modulated signal measurements, the proposed CM-LMBA also showed good linearity with and without DPD correction, achieving excellent average efficiency. The Simulation and experimental results validated the broadband and high-efficiency performance of the proposed CM-LMBA architecture.

References

[1] P. Chen and S. He, "Investigation of inverse class-E power amplifier at sub-nominal condition for any duty ratio," *IEEE Trans. Circuits Syst. I Reg. Papers*, vol. 62, no. 4, pp. 1015–1024, Apr. 2015.

[2] S. C. Cripps, P. J. Tasker, A. L. Clarke, J. Lees, and J. Benedikt, "On the continuity of high efficiency modes in linear rf power amplifiers," *IEEE Microw. Wirel. Compon. Lett.*, vol. 19, no. 10, pp. 665–667, Oct. 2009.

[3] C. Li, F. You, S. He, X. Tang, W. Shi, and J. Wang, "High-efficiency power amplifier employing minimum-power harmonic active load modulator," *IEEE Trans. Circuits Syst. II Express Briefs*, vol. 66, no. 8, pp. 1371–1375, Aug. 2019.

[4] K. Chen and D. Peroulis, "Design of broadband highly efficient harmonic-tuned power amplifier using in-band continuous class-F/F^{-1} mode transferring," *IEEE Trans. Microw. Theory Techn.*, vol. 60, no. 12, pp. 4107–4116, Dec. 2012.

[5] X. Y. Zhou, S. Y. Zheng, W. S. Chan, S. Chen, and D. Ho, "Broadband efficiency-enhanced mutually coupled harmonic postmatching Doherty power amplifier," *IEEE Trans. Circuits Syst. I Reg. Papers*, vol. 64, no. 7, pp. 1758–1771, Jul. 2017.

[6] J. Pang, S. He, C. Huang, Z. Dai, J. Peng, and F. You, "A post-matching Doherty power amplifier employing low-order impedance inverters for broadband applications," *IEEE Trans. Microw. Theory Techn.*, vol. 63, no. 12, pp. 4061–4071, Dec. 2015.

[7] X. Y. Zhou, S. Y. Zheng, W. S. Chan, X. Fang, and D. Ho, "Postmatching Doherty power amplifier with extended back-off range based on self-generated harmonic injection," *IEEE Trans. Microw. Theory Techn.*, vol. 66, no. 4, pp. 1951–1963, Apr. 2018.

[8] Z. Yang, Y. Yao, M. Li, Y. Jin, T. Li, Z. Dai, F. Tang, and Z. Li, "Bandwidth extension of Doherty power amplifier using complex combining load with noninfinity peaking impedance," *IEEE Trans. Microw. Theory Tech.*, vol. 67, no. 2, pp. 765–777, Feb. 2019.

[9] W. Shi, S. He, F. You, H. Xie, G. Naah, Q. Liu, and Q. Li, "The influence of the output impedances of peaking power amplifier on broadband Doherty amplifiers," *IEEE Trans. Microw. Theory Techn.*, vol. 65, no. 8, pp. 3002–3013, Aug. 2017.

[10] X. Y. Zhou, W. S. Chan, S. Y. Zheng, W. Feng, H. Liu, K. M. Cheng, and D. Ho, "A mixed topology for broadband high-efficiency Doherty power amplifier," *IEEE Trans. Microw. Theory Techn.*, vol. 67, no. 3, pp. 1050–1064, Mar. 2019.

[11] J. Pang, S. He, Z. Dai, C. Huang, J. Peng, and F. You, "Design of a post-matching asymmetric Doherty power amplifier for broadband applications," *IEEE Microw. Wirel. Compon. Lett.*, vol. 26, no. 1, pp. 52–54, Jan. 2016.

[12] G. Lv, W. Chen, X. Chen, F. M. Ghannouchi, and Z. Feng, "A compact Ka/Q dual-band GaAs mmic Doherty power amplifier with simplified offset lines for 5G applications," *IEEE Trans. Microw. Theory Techn.*, vol. 67, no. 7, pp. 3110–3121, Jul. 2019.

[13] X. Fang, H. Liu, and K. M. Cheng, "Extended efficiency range, equal-cell Doherty amplifier design using explicit circuit model," *IEEE Microw. Wirel. Compon. Lett.*, vol. 27, no. 5, pp. 497–499, May 2017.

[14] J. Xia, M. Yang, Y. Guo, and A. Zhu, "A broadband high-efficiency Doherty power amplifier with integrated compensating reactance," *IEEE Trans. Microw. Theory Techn.*, vol. 64, no. 7, pp. 2014–2024, Jul. 2016.

[15] G. Lv, W. Chen, X. Liu, F. M. Ghannouchi, and Z. Feng, "A fully integrated C-band GaN MMIC Doherty power amplifier with high efficiency and compact size for 5G application," *IEEE Access*, vol. 7, pp. 71 665–71 674, Apr. 2019.

[16] X. Fang, H. Liu, K. M. Cheng, and S. Boumaiza, "Modified Doherty Amplifier With Extended Bandwidth and Back-Off Power Range Using Optimized Peak Combining Current Ratio," *IEEE Trans. Microw. Theory Techn.*, vol. 66, no. 12, pp. 5347–5357, Dec. 2018.

[17] M. Li, J. Pang, Y. Li, and A. Zhu, "Ultra-wideband dual-mode Doherty power amplifier using reciprocal gate bias for 5G applications," *IEEE Trans. Microw. Theory Techn.*, vol. 67, no. 10, pp. 4246–4259, Oct. 2019.

[18] J. Pang, Y. Li, M. Li, Y. Zhang, X. Y. Zhou, Z. Dai, and A. Zhu, "Multiband dual-mode Doherty power amplifier employing phase periodic matching network and reciprocal gate bias for 5g applications," *IEEE Trans. Microw. Theory Techn.*, pp. 1–13, Feb. 2020.

[19] D. J. Shepphard, J. Powell, and S. C. Cripps, "An efficient broadband reconfigurable power amplifier using active load modulation," *IEEE Microw. Wirel. Compon. Lett.*, vol. 26, no. 6, pp. 443–445, Jul. 2016.

[20] P. H. Pednekar, E. Berry, and T. W. Barton, "RF-input load modulated balanced amplifier with octave bandwidth," *IEEE Trans. Microw. Theory Techn.*, vol. 65, no. 12, pp. 5181–5191, Dec. 2017.

[21] R. Quaglia and S. Cripps, "A load modulated balanced amplifier for telecom applications," *IEEE Trans. Microw. Theory Techn.*, vol. 66, no. 3, pp. 1328–1338, Mar. 2018.

[22] T. Cappello, P. Pednekar, C. Florian, S. Cripps, Z. Popovic, and T. W. Barton, "Supply- and load-modulated balanced amplifier for efficient broadband 5g base stations," *IEEE Trans. Microw. Theory Techn.*, vol. 67, no. 7, pp. 3122–3133, Jul. 2019.

[23] P. H. Pednekar, W. Hallberg, C. Fager, and T. W. Barton, "Analysis and design of a Doherty-like RF-input load modulated balanced amplifier," *IEEE Trans. Microw. Theory Techn.*, vol. 66, no. 12, pp. 5322–5335, Dec. 2018.

[24] T. Cappello, P. H. Pednekar, C. Florian, Z. Popovic, and T. W. Barton, "Supply modulation of a broadband load modulated balanced amplifier," in *2018 IEEE MTT-S International Microwave Symposium (IMS)*, Jun. 2018, pp. 304–307.

[25] J. R. Powell, D. J. Shepphard, R. Quaglia, and S. C. Cripps, "A power reconfigurable high-efficiency X -band power amplifier mmic using the load modulated balanced amplifier technique," *IEEE Microw. Wirel. Compon. Lett.*, vol. 28, no. 6, pp. 527–529, Jun. 2018.

[26] H. Lyu and K. Chen, "Balanced-to-Doherty mode-reconfigurable power amplifier with high efficiency and linearity against load mismatch," *IEEE Trans. Microw. Theory Techn.*, vol. 68, no. 5, pp. 1717–1728, May 2020.

[27] P. Saad, R. Hou, R. Hellberg, and B. Berglund, "An 80W power amplifier with 50% efficiency at 8 dB power back-off over 2.6-3.8 GHz," in *2019 IEEE MTT-S International Microwave Symposium(IMS)*, Jul. 2019, pp. 1328–1330.

[28] ——, "The continuum of load modulation ratio from Doherty to traveling-wave amplifiers," *IEEE Trans. Microw. Theory Tech.*, pp. 1–13, Oct. 2019.

[29] X. Chen, W. Chen, F. M. Ghannouchi, Z. Feng, and Y. Liu, "A broadband Doherty power amplifier based on continuous-mode technology," *IEEE Trans. Microw. Theory Techn.*, vol. 64, no. 12, pp. 4505–4517, Dec. 2016.

[30] W. Shi, S. He, X. Zhu, B. Song, Z. Zhu, G. Naah, and M. Zhang, "Broadband continuous-mode Doherty power amplifiers with noninfinity peaking impedance," *IEEE Trans. Microw. Theory Techn.*, vol. 66, no. 2, pp. 1034–1046, Feb. 2018.
[31] J. Pang, Y. Li, M. Li, Y. Zhang, X. Y. Zhou, Z. Dai, and A. Zhu, "Analysis and design of highly efficient wideband RF-input sequential load modulated balanced power amplifier," *IEEE Trans. Microw. Theory Techn.*, pp. 1–13, Jan. 2020.
[32] Y. Cao, H. Lyu, and K. Chen, "Load modulated balanced amplifier with reconfigurable phase control for extended dynamic range," in *2019 IEEE MTT-S International Microwave Symposium (IMS)*, Jun. 2019, pp. 1335–1338.
[33] Y. Cao and K. Chen, "Pseudo-Doherty load-modulated balanced amplifier with wide bandwidth and extended power back-off range," *IEEE Trans. Microw. Theory Techn.*, pp. 1–1, Jun. 2020.
[34] J. Pang, S. He, Z. Dai, C. Huang, J. Peng, and F. You, "Novel design of highly-efficient concurrent dual-band GaN Doherty power amplifier using direct-matching impedance transformers," in *2016 IEEE MTT-S International Microwave Symposium (IMS)*, May 2016, pp. 1–4.
[35] ——, "Design of continuous-mode GaN power amplifier with compact fundamental impedance solutions on package plane," *Antennas Propag. IET Microw.*, vol. 10, no. 10, pp. 1056–1064, Jul. 2016.
[36] N. Tuffy, L. Guan, A. Zhu, and T. J. Brazil, "A simplified broadband design methodology for linearized high-efficiency continuous class-F power amplifiers," *IEEE Trans. Microw. Theory Techn.*, vol. 60, no. 6, pp. 1952–1963, Jun. 2012.
[37] T. Canning, P. J. Tasker, and S. C. Cripps, "Continuous mode power amplifier design using harmonic clipping contours: Theory and practice," *IEEE Trans. Microw. Theory Techn.*, vol. 62, no. 1, pp. 100–110, Jan. 2014.
[38] S. Rezaei, L. Belostotski, M. Helaoui, and F. M. Ghannouchi, "Harmonically tuned continuous class-c operation mode for power amplifier applications," *IEEE Trans. Microw. Theory Techn.*, vol. 62, no. 12, pp. 3017–3027, Dec. 2014.
[39] J. Xia, W. Chen, F. Meng, C. Yu, and X. Zhu, "Improved three-stage Doherty amplifier design with impedance compensation in load combiner for broadband applications," *IEEE Trans. Microw. Theory Tech.*, vol. 67, no. 2, pp. 778–786, Feb. 2019.
[40] H. Chang, Y. Hahn, P. Roblin, and T. W. Barton, "New mixed-mode design methodology for high-efficiency outphasing chireix amplifiers," *IEEE Trans. Circuits Syst. Regul. Pap.*, vol. 66, no. 4, pp. 1594–1607, Apr. 2019.
[41] Y. Li, W. Cao, and A. Zhu, "Instantaneous sample indexed magnitude-selective affine function-based behavioral model for digital predistortion of RF power amplifiers," *IEEE Trans. Microw. Theory Techn.*, vol. 66, no. 11, pp. 5000 – 5010, Nov. 2018.

Jingzhou Pang (S'13-M'16) received the B.S. degree in electrical engineering and Ph. D. degree in circuits and systems from University of Electronic Science and Technology of China (UESTC), Chengdu, China, in 2010 and 2016, respectively. In December 2016, he joined Huawei Technologies Company Ltd., Shenzhen, China, where he was a engineer in charge of the research and development of 5G high efficiency power amplifiers and transmitters. He is currently with the RF and Microwave Research Group at University College Dublin (UCD), Dubin, Ireland, as a research fellow. His research interests include broadband high-efficiency power amplifier systems, bandwidth extension techniques for high-efficiency transmitters and MMIC power amplifier design for RF/microwave and millimeter-wave applications.

Jingzhou Pang was a recipient of the EDGE Marie Sklodowska-Curie Individual Fellowship. He was a recipient of third Place Award of the High Efficiency Power Amplifier Student Design Competition, IEEE Microwave Theory and Techniques Society (IEEE MTT-S) International Microwave Symposium (IMS) in 2013.

Chenhao Chu (S'19) received the B.E. degree from Nanjing University of Science and Technology, Nanjing, China, in 2015, and the M.S. degree (Hons.) from City University of Hong Kong, Hong Kong, China, in 2017. From Oct. 2017 to Sept. 2018, he was a Research Assistant with the State Key Laboratory of Millimeter Waves, Department of Electronic Engineering, City University of Hong Kong.

Currently, he is pursuing Ph.D. degree in the RF and Microwave Research Group at University College Dublin, Dublin, Ireland. His research interests include broadband high-efficiency power amplifiers, MMIC power amplifier design for RF/microwave and millimeter-wave applications and antenna-in-package at mm-Waves.

Yue Li (S'17) received the B.E. degree in information engineering from Southeast University, Nanjing, China, in 2016. He is currently working towards the Ph.D. degree at University College Dublin, Dublin, Ireland.

He is currently with the RF and Microwave Research Group, UCD. His current research interests include behavioral modeling and digital predistortion for RF power amplifiers.

Anding Zhu (S'00-M'04-SM'12) received the Ph.D. degree in electronic engineering from University College Dublin (UCD), Dublin, Ireland, in 2004.

He is currently a Professor with the School of Electrical and Electronic Engineering, UCD. His research interests include high-frequency nonlinear system modeling and device characterization techniques, high-efficiency power amplifier design, wireless transmitter architectures, digital signal processing, and nonlinear system identification algorithms. He has published more than 130 peer-reviewed journal and conference articles.

Prof. Zhu is an elected member of MTT-S AdCom, the Chair of the Electronic Information Committee and the Vice Chair of the Publications Committee. He is also the Chair of the MTT-S Microwave High-Power Techniques Committee. He served as the Secretary of MTT-S AdCom in 2018. He was the General Chair of the 2018 IEEE MTT-S International Microwave Workshop Series on 5G Hardware and System Technologies (IMWS-5G) and a Guest Editor of the IEEE TRANSACTIONS ON MICROWAVE THEORY AND TECHNIQUES on 5G Hardware and System Technologies. He is currently an Associate Editor of the IEEE Microwave Magazine and a Track Editor of the IEEE TRANSACTIONS ON MICROWAVE THEORY AND TECHNIQUES.